Accuracy-ensured Impedance Scanning: Error Analysis on Frequency Step and Perturbation Amplitude

Yang Zhu, Siqi Bu*
Department of Electrical and Electronic Engineering
The Hong Kong Polytechnic University
Hong Kong SAR, China
yang-zy.zhu@connect.polyu.hk, siqi.bu@polyu.edu.hk

Ilhan Kocar
Department of Electrical Engineering
Polytechnique Montreal
Montreal, Canada
ilhan.kocar@polymtl.ca

***Abstract*—Electromagnetic transient (EMT)–based frequency scanning has become a promising tool for extracting black-box impedance models of inverter-based resources (IBRs) in small-signal stability assessment. However, the selection of frequency step size and perturbation amplitude is often heuristic. This paper systematically investigates how these two configuration parameters influence impedance accuracy and Nyquist-based stability assessment. First, analytical expressions are derived to relate the impedance magnitude error to the frequency step and the resonant bandwidth, showing that the error near narrow resonances increases quadratically with the normalized step size. Next, the error due to perturbation amplitude is examined by combining a small-signal nonlinearity expansion with a signal-to-noise-ratio (SNR) argument, yielding a composite error model that increases for both excessively small and excessively large amplitudes. The implications of these errors for Nyquist-based stability assessment are then analyzed, revealing potential risks of stability misjudgment. Case studies on a grid-following IBR validate the analytical trends and provide practical guidelines for selecting frequency steps and perturbation amplitudes to ensure reliable impedance-based stability assessment.**

***Index Terms*—Frequency scanning, inverter-based resources, frequency step, perturbation amplitude, impedance-based stability assessment.**

I. Introduction

With the rapidly growing penetration of inverter-based resources (IBRs), the risk of system instability is also increasing. Consequently, impedance-based small-signal stability analysis [1] has become a widely used method for assessing converter-grid interactions due to its simplicity and broad applicability. In practice, however, the internal control structures and algorithms of commercial IBRs are typically not disclosed for proprietary reasons; therefore, the electromagnetic transient (EMT)-based frequency-scanning techniques are widely employed to obtain their black-box dynamic characteristics [2], [3].

While existing research has extensively investigated frequency-scanning techniques across various reference frames, including the positive-sequence, αβ, and dq frames, and has compared their computational efficiency and accuracy [4], [5], little attention has been paid to the reliability of the impedance measurement itself. Specifically, how the configuration of the frequency scanning affects the accuracy of the measured impedance and the subsequent stability assessment has not been systematically analyzed. Among these configurable settings—such as perturbation type [6], injection method, frequency step, and perturbation amplitude—the frequency step and perturbation amplitude are the most commonly available and adjustable parameters in both user-developed tools and commercial software, yet their selection is often empirical [7]. Although guidance on perturbation amplitude is provided in [8], [9], the underlying mechanisms of measurement error and their impact on stability assessment have not been investigated, and the effect of frequency step has been seldom studied. The lack of quantitative understanding and clear configuration guidelines for these two parameters can result in inaccurate or misleading conclusions in impedance-based stability assessment, particularly near the system's stability boundary.

This paper addresses the above methodological gap by answering a simple yet practically important question: How do the frequency step size and perturbation amplitude of EMT-based frequency scanning affect the reliability of impedance-based stability assessment, and how should they be chosen in practice?

The main contributions are summarized as follows:

1. Mechanistic insight: Analytical expressions are derived to quantify the effects of frequency step and perturbation amplitude on impedance measurement errors, providing the first systematic and quantitative understanding of these error mechanisms.
2. Stability interpretation: The measurement errors are incorporated into the Nyquist-based stability analysis, first clearly revealing how such errors distort distance margins and can lead to stability-assessment misjudgment.
3. Practical guidelines: A comprehensive case study quantifies the impact of frequency-scanning configuration and delivers practical guidance on selecting frequency step and perturbation amplitude for reliable impedance measurement.

979-8-3315-8138-1

The remainder of the paper is organized as follows. Section II presents the principle of frequency scanning. Section III analyzes the error mechanisms associated with the frequency step and perturbation amplitude. Section IV examines their impact on stability assessment. Section V presents a case study of a grid-following IBR system, and Section VI provides practical guidelines for reliable frequency scanning. Section VII concludes the paper.

II. PRINCIPLE OF EMT-BASED FREQUENCY SCANNING

To illustrate EMT-based frequency scanning, the system depicted in Fig. 1 is employed.

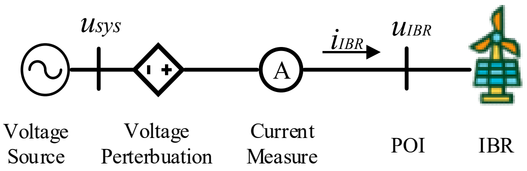

Fig. 1. Schematic diagram of p-scan using voltage perturbation injection.

As an example, the positive-sequence scan (p-scan) is considered. Once the IBR reaches steady-state, a small balanced three-phase voltage perturbation in the positive sequence at frequency f_p is superimposed on the fundamental voltage. The perturbation amplitude, denoted as A, is typically specified as a percentage of the nominal voltage. The resulting three-phase current at the point of interconnection (POI) is then measured and recorded over multiple cycles after system transients have decayed. The frequency spectra of the measured signals are then extracted using the fast Fourier transform (FFT) or other suitable methods. Subsequently, the impedance of the IBR at frequency f_p is calculated as:

$$Z_{IBR}(f_p) = \frac{U_{IBR}(f_p)}{I_{IBR}(f_p)} \tag{1}$$

The procedure is repeated for each perturbation frequency of interest within the specified frequency range, which can be expressed as:

$$f_p = f_{\min} + k\Delta f, k = 0,1,...,N \tag{2}$$

where Δf is the frequency step and N represents the number of frequency-scan points.

In practice, the selection of Δf and A often vary across users, which may lead to inconsistent impedance spectra and potentially inaccurate or even conflicting stability assessments. The following section analyzes their effects on measurement errors in detail.

III. ERROR MECHANISM ANALYSIS

This section presents the analytical derivation of measurement errors associated with the frequency step and perturbation amplitude, providing a quantitative explanation of their underlying impact on the extracted impedance. The impedance obtained from EMT-based frequency scan can be expressed as follows:

$$\hat{Z}(j\omega) = Z(j\omega) + \Delta Z(j\omega) \tag{3}$$

where Z(jw) denotes the true small-signal impedance, $\hat{Z}(jw)$ represents the measured value, and ΔZ(jw) quantifies the measurement error.

A. Errors Associated with Frequency Step

In the small-signal range, the IBR can be linearized into a linear model, in which each oscillatory mode corresponds to a complex-conjugate eigenvalue pair. In a narrow frequency neighborhood around a poorly damped resonance where one mode is dominant, the local frequency response is dominated by the corresponding complex-conjugate pair; therefore, the impedance magnitude can be locally approximated by a standard second-order form [10], given by:

$$|Z(j\omega)| \approx \frac{Z_r}{\sqrt{\left(1-\left(\frac{\omega}{\omega_r}\right)^2\right)^2 + \left(2\zeta\frac{\omega}{\omega_r}\right)^2}} \tag{4}$$

where $Z_r = |Z_r(j\omega_r)|$ denotes the peak magnitude at resonant frequency ω_r, ζ is the damping ratio, and bandwidth $B_w \approx 2\zeta\omega_r$.

Applying a second-order Taylor expansion at $\omega = \omega_r$ yields a local quadratic approximation:

$$|Z(j\omega)| \approx Z_r - \frac{1}{2}\alpha\frac{Z_r}{B_\omega^2}(\omega-\omega_r)^2 \tag{5}$$

where α is an order-one constant determined by the second derivative at the peak. The detailed derivation follows directly from a Taylor expansion and is omitted here for brevity.

In a discrete frequency scan with step size $\Delta\omega = 2\pi\Delta f$, the maximum measured magnitude near the resonance ω_r is taken at the nearest point ω_{k*}, which satisfies:

$$|\omega_{k*} - \omega_r| \le \frac{\Delta\omega}{2} \tag{6}$$

Accordingly, the relative peak error can be approximated as:

$$\frac{|\Delta Z_{\text{step}}|}{Z_r} \approx C_f\left(\frac{\Delta\omega}{B_\omega}\right)^2 = C_f\left(\frac{\Delta f}{B_f}\right)^2 \tag{7}$$

$$|\Delta Z_{\text{step}}| = Z_r - |Z(j\omega_{k*})| \tag{8}$$

where $C_f = \alpha/8$ is another order-one constant, and $B_f = B_\omega/2\pi$ represents the bandwidth in Hz, and $|\Delta Z_{\text{step}}|$ denotes the measurement error associated with frequency step Δf.

It is evident that the measurement error exhibits a quadratic dependence on the normalized frequency step $\Delta f / B_f$. Moreover, narrow-band modes are more sensitive to coarse frequency steps.

B. Errors Associated with Pertebation Amplitude

The selection of the perturbation amplitude A is not straightforward: an amplitude that is too small results in a low signal-to-noise ratio (SNR), while an amplitude that is too large may violate the linearity. Both cases introduce measurement errors. Therefore, the error mechanisms will be analyzed from the perspectives of SNR and nonlinearity.

First, the measurement error caused by the SNR is analyzed. Taking the voltage perturbation injection described in Section II as an example, the perturbation voltage is denoted by $u(t)=A\sin(\omega t)$, while $\tilde{V}(j\omega)$ represents its phasor form. The measured current phasor $\tilde{I}_m(j\omega)$ can then be expressed as:

$$\tilde{I}_m(j\omega)=\tilde{I}(j\omega)+n(j\omega) \tag{9}$$

where $\tilde{I}(j\omega)$ denotes true linear response current phasor, and $n(j\omega)$ represents the noise which mainly arises from numerical sampling errors, FFT spectral leakage, and harmonics generated by power electronic switching. The impedance can be expressed as:

$$\hat{Z}(j\omega)=\frac{\tilde{V}(j\omega)}{\tilde{I}(j\omega)+n(j\omega)} \tag{10}$$

If $\left|n(j\omega)/\tilde{I}(j\omega)\right|<<1$, the impedance expression can be expanded using a first-order Taylor approximation, leading to the following error formulation:

$$\begin{gathered}\frac{|\Delta Z_{nosise}|}{|Z_1|}\approx\frac{|n(j\omega)|}{\left|\tilde{I}(j\omega)\right|}=\frac{1}{SNR}\\ Z_1(j\omega)=\tilde{V}(j\omega)/\tilde{I}(j\omega)\end{gathered} \tag{11}$$

Since the noise is independent of the perturbation amplitude A, and A remains sufficiently small in the SNR analysis such that linearity is preserved, the true current response $\tilde{I}(j\omega)$ is proportional to the perturbation amplitude A. Therefore:

$$\frac{|\Delta Z_{nosise}|}{|Z_1|}\propto\frac{1}{A},thus\frac{|\Delta Z_{nosise}|}{|Z_1|}=C_2\frac{1}{A} \tag{12}$$

where C_2 denotes the lumped proportionality constant associated with the measurement noise at the injected frequency. It can be observed that an excessively small perturbation amplitude leads to a significant measurement error.

In contrast, when the perturbation amplitude A becomes excessively large, the IBR may no longer operate within its linear small-signal region. In this case, the measured current contains nonlinear distortion components, which bias the extracted impedance. The measured current phasor $\tilde{I}_m(j\omega)$ is expressed as:

$$\tilde{I}_m(j\omega)=\tilde{I}(j\omega)+\tilde{I}_{nl}(j\omega) \tag{13}$$

where $\tilde{I}_{nl}(j\omega)$ represents the nonlinear current component, which is associated with control saturation or PLL coupling.

Expanding $\tilde{I}_m(j\omega)$ with respect to the perturbation amplitude A around the operating point $A=0$ yields

$$\tilde{I}_m(j\omega)=Y_1(j\omega)A+\frac{1}{6}Y_3(j\omega)A^3+O(A^5) \tag{14}$$

Where $Y_1(j\omega)$ is the true linear admittance and $Y_3(j\omega)$ denotes the first nonlinear distortion component. Only odd-order nonlinear terms appear in the Taylor expansion because the even-order terms do not contribute to $\tilde{I}_m(j\omega)$ at frequency ω. Since $\tilde{V}(j\omega)\propto A$, the impedance can be expressed as:

$$\begin{aligned}\hat{Z}(j\omega)&=\frac{\tilde{V}(j\omega)}{\tilde{I}_m(j\omega)}=\frac{1}{Y_1(j\omega)+\frac{1}{6}Y_3(j\omega)A^2+O(A^4)}\\ &\approx\frac{1}{Y_1(j\omega)}\left[1-\frac{1}{6}\frac{Y_3(j\omega)}{Y_1(j\omega)}A^2\right]\end{aligned} \tag{15}$$

Then, the error can be expressed as:

$$\frac{|\Delta Z_{nonlinear}|}{|Z_1|}\approx\frac{1}{6}\left|\frac{Y_3(j\omega)}{Y_1(j\omega)}\right|A^2\propto A^2 \tag{16}$$

It can be clearly observed that once linearity is violated, the resulting error grows quadratically with the perturbation amplitude.

The overall impedance measurement errors associated with the perturbation amplitude can be summarized as:

$$\begin{gathered}\frac{|\Delta Z_{amplitude}|}{|Z_1|}\approx C_1A^2+C_2\frac{1}{A}\\ C_1=\frac{1}{6}|Y_3(j\omega)|/|Y_1(j\omega)|\end{gathered} \tag{17}$$

It is worth noting that the frequency step induced error is a local effect that appears only around modal resonances. In contrast, the perturbation amplitude induced error is a global effect, since both nonlinear distortion and noise sensitivity propagate over the entire spectrum. Therefore, the total error can be expressed as:

$$\frac{|\Delta Z|}{|Z|}\approx C_f\left(\frac{\Delta f}{B_f}\right)^2+C_1A^2+C_2\frac{1}{A} \tag{18}$$

where the first term is restricted to narrow-band resonance regions, while the latter two terms influence the entire scanned spectrum. Eq. (18) summarizes the dominant error mechanisms and their scaling trends with respect to Δf and A; the coefficients are implementation-dependent, and thus the model is primarily used for trend analysis rather than point-by-point absolute error prediction.

IV. Impact on Nyquist-Based Stability Assessment

Since Nyquist-based stability assessment depends on the impedance of the gird and IBR, any measurement error from frequency scanning will degrade the accuracy of the stability analysis.

For a grid connected IBR, the loop gain can be expressed as:

$$L(j\omega)=Z_{Grid}(j\omega)/Z_{IBR}(j\omega) \tag{19}$$

When analyzing the impact of IBR impedance measurement error, the grid-side impedance can be regarded as fixed. Therefore, the relationship between the loop-gain error and the IBR impedance error can be derived as follows:

$$\frac{\Delta L}{L}\approx-\frac{\Delta Z_{IBR}}{Z_{IBR}} \tag{20}$$

The true and measured minimum distance of the Nyquist curve to the critical point (-1, j0) are defined as:

$$d_{\min} = \min_{\omega}\left|1+L(j\omega)\right|, \hat{d}_{\min} = \min_{\omega}\left|1+\hat{L}(j\omega)\right| \qquad (21)$$

The deviation between the measured and true minimum distances can then be derived as:

$$\left|\hat{d}_{\min} - d_{\min}\right| \le \max_{\omega}\left|\hat{L}(j\omega) - L(j\omega)\right| = \max_{\omega}\left|\Delta L\right| \approx \max_{\omega}\left|L\right|\left|\frac{\Delta Z_{IBR}}{Z_{IBR}}\right| \qquad (22)$$

Based on this, two conclusions can be drawn:

Conclusion 1: if the loop-gain deviation satisfies $\max_{\omega}|\Delta L| < d_{\min}$, the Nyquist-based stability judgment is guaranteed to be correct, and no misclassification will occur. This condition is sufficient for ensuring reliable stability assessment.

Conclusion 2: The essence of ensuring reliable stability judgment lies in the comparison between the loop-gain deviation and the true minimum distance $d_{\min}$. Thus, neither a large impedance error nor a large loop-gain alone is sufficient to determine whether the stability assessment will be correct.

V. Case Study

This section presents a case study in DIgSILENT PowerFactory to illustrate the proposed error mechanism and its impact on impedance-based stability assessment. The test system consists of an IBR connected to an equivalent grid impedance, as shown in Fig. 2. Due to space limitations, only grid-following IBRs are considered in this paper. The detailed system parameters are listed in TABLE I.

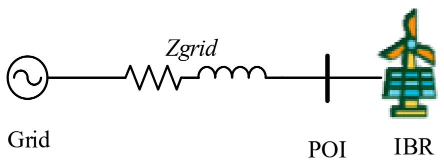

Fig. 2. Diagram of the test system.

TABLE I. Parameters of The Test System

Item	symbolic	value
System frequency	f_b	50 Hz
Voltage base	V_{base}	0.69 kV
Power base	S_{base}	1.66 MVA
Frequency scan range	f_p	1 - 100 Hz
System strength	SCR	1.81
Power level	P_{PoI} / Q_{PoI}	1.0 p.u. / 0 p.u.
Grid side impedance	X/R	10
	Z_{grid}	0.0157+j0.157Ω

The scan range is set to 1–100 Hz, which covers the sub-synchronous oscillation region. The configurations of all test cases are listed in TABLE II. Since the IBR is treated as a black box, its analytical impedance is unavailable. A high-resolution scan R (Δf = 0.5 Hz, A = 0.1%) is therefore used as a best-available benchmark for comparison when analytical models are inaccessible. It adopts the finest step used in this study and a small perturbation amplitude to reduce discretization and nonlinear distortion while maintaining adequate SNR and reasonable EMT simulation time.

TABLE II. Configuration of All Test Cases

Case	Frequency Step (Δf / Hz)	Perturbation Amplitude (A / %)
R	0.5	0.1
F0	0.5	0.5
F1	1	0.5
F2	5	0.5
F3	10	0.5
A0	1	0.1
A1	1	0.5
A2	1	1
A3	1	5

A. Freqency Step Study

In this part, 0.5% amplitude is verified to be in the linear region by comparing F0 with the benchmark case R; their frequency responses coincide. F0 is therefore used as the reference for subsequent frequency-step analysis, so that the perturbation amplitude is fixed and only Δf varies across F0–F3. Fig. 3 shows the bode plots and TABLE III summarizes the maximum impedance errors.

The largest errors (up to 99.84%) occur around 50-60 Hz, where the IBR exhibits a weakly damped resonance, which is consistent with the error mechanism derived in (7). Fig. 4 presents the Nyquist plots, and TABLE IV summarizes the stability analysis results.

The minimum Nyquist distance is only weakly affected by Δf, and Δd remains small, so the stability assessment remains consistent across F0–F3 despite the extremely large impedance errors near the resonance band. Moreover, (22) is verified in all cases, i.e., $\Delta d \le \max_{\omega}|\Delta L|$. However, the sufficient condition in ***Conclusion 1***, $\max_{\omega}|\Delta L| < d_{\min}$ is not satisfied because $\max_{\omega}|\Delta L|$ occurs in the resonance band (e.g., 0.1687@61.5 Hz, 1.952@51 Hz, 0.851@50.5Hz) whereas the $d_{\min}$ frequency remains at 82.5 Hz. This highlights the conservative nature of ***Conclusion 1*** and supports ***Conclusion 2*** that the judgement reliability is governed by the loop-gain deviation relative to the true minimum distance $d_{\min}$.

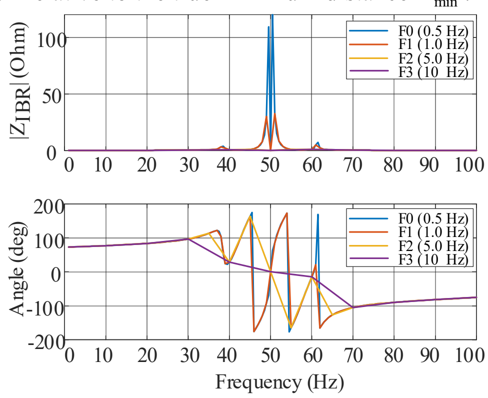

Fig. 3. Bode plots of cases with different frequency steps.

TABLE III. Maximum Impedance Error vs. Frequency Step

Case	Magnitude Error		Phase Error	
	Max ΔZ/Z	f_{max} (Hz)	Max Δθ (°)	f_{max} (Hz)
F1	83.03%	50.5	140.31	61.5
F2	99.88%	50.5	166.79	61.5
F3	99.84%	50.5	178.64	47.0

979-8-3315-8138-1

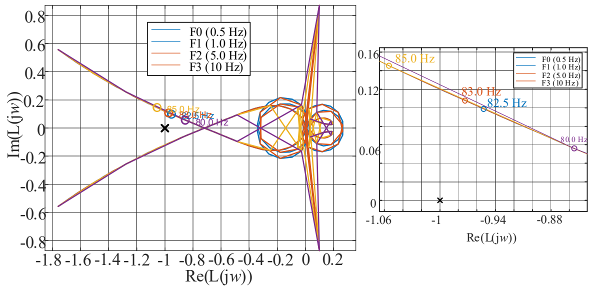

Fig. 4. Nyquist plots of cases with different frequency steps.

TABLE IV. MINIMUM DISTANCE TO (-1, j0) VS. FREQUENCY STEP

Case	$d_{\min}$	$\hat{d}_{\min}$	Δd	$f_{d\min}$ (Hz)	$\max_{\omega}\lvert\Delta L\rvert$	$f_{\Delta L\max}$ (Hz)	Assessment
F0	0.1095			82.5			Stable
F1	0.1095	0.1111	0.0016	83	0.1687	61.5	Stable
F2	0.1095	0.1556	0.0461	85	1.952	51.0	Stable
F3	0.1095	0.1557	0.0462	80	0.851	50.5	Stable

B. Perturbation Amplitude Study

In this part, A0 (Δf=1 Hz, A = 0.1%) is used as reference. Here, Δf is fixed at 1 Hz for all amplitude cases (A0–A3) to isolate the impact of A and to keep the EMT scanning effort tractable. The reference amplitude A = 0.1% provides a low-distortion baseline within the identified linear region. Fig. 5 shows the bode and Nyquist plots, and TABLE V summarizes the maximum impedance errors. The impedance error increases nearly quadratically with A from 1% (A2) to 5% (A3), confirming the nonlinear distortion predicted in (16). Nevertheless, the $\hat{d}_{\min}$ remains almost unchanged across all cases, and all cases are stable. Furthermore, the sufficient condition in ***Conclusion 1*** is satisfied for all cases, i.e., $\max_{\omega}\lvert\Delta L\rvert < d_{\min}$. Specifically, $\max_{\omega}\lvert\Delta L\rvert$ = 0.0497 (A1), 0.0566 (A2), and 0.0833 (A3), all below $d_{\min}$ = 0.1111. Therefore, in this study, ***Conclusion 1*** provides a worst-case guarantee for reliable stability assessment.

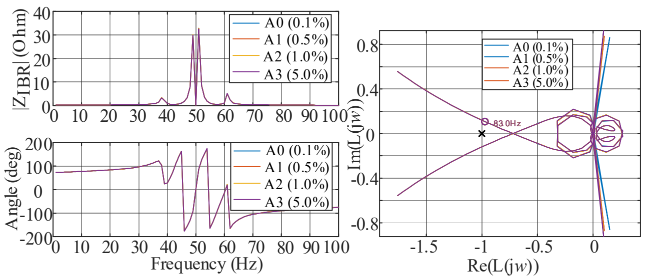

Fig. 5. Bode plots (left) and Nyquist plots (right) under different amplitudes.

TABLE V. MAXIMUM IMPEDANCE ERROR VS. PERTURBATION AMPLITUDE

Case	Magnitude Error		Phase Error	
	Max ΔZ/Z	f_{max} (Hz)	Max Δθ (°)	f_{max} (Hz)
A1	0.37%	45	3.25	50
A2	0.85%	50	3.66	50
A3	5.90%	50	3.98	50

VI. PRACTICAL GUIDELINES

For EMT-based frequency scanning of grid-following IBRs in the 1–100 Hz sub-synchronous range, two practical configuration guidelines are recommended (see TABLE VI).

First, the frequency step should be sufficiently smaller than the narrowest resonance bandwidth, as illustrated in (7). When prior system knowledge is limited, resonant regions (and an effective bandwidth estimate) can be identified via a two-stage scan: perform an initial coarse scan and then locally refine the step around detected resonance peaks.

Second, the perturbation amplitude should remain within the linear small-signal region while ensuring adequate SNR, as illustrated in (17). In the tested system, a wide linear region is observed, and a default amplitude provides a robust compromise, whereas overly large amplitudes may activate nonlinear behavior and should be avoided (see TABLE VI). This setting is intended for offline/open-loop IBR scanning; for grid-connected (closed-loop) frequency scanning, the admissible amplitude should also satisfy current/voltage limits and may depend on grid strength (e.g., SCR).

TABLE VI. RECOMMEND SCANNING SETTINGS (1–100 HZ)

Item	Recommendation
Frequency Step Δf	1 Hz (global), refine to 0.5 Hz near resonances
Perturbation Amplitude A	0.1%–1% (default 0.5%), avoid ≥5%

VII. CONCLUSION

This paper analyzes how the frequency step and perturbation amplitude affect EMT-based impedance scanning accuracy and the resulting Nyquist-based stability assessment. Practical recommendations are summarized in TABLE VI, and a robustness condition to prevent stability misjudgment is established. The case studies focus on a grid-following IBR; however, the error mechanism introduced by finite frequency steps is generic and the same configuration logic is expected to apply to grid-forming or hybrid controls, for which the admissible perturbation amplitude range should be re-identified due to different nonlinearities and limiters.

REFERENCES

[1] J. Sun, "Impedance-Based Stability Criterion for Grid-Connected Inverters," *IEEE Trans. Power Electron.*, vol. 26, no. 11, pp. 3075-3078, Nov. 2011.

[2] L. Fan, Z. Miao, P. Koralewicz, S. Shah, and V. Gevorgian, "Identifying DQ-Domain Admittance Models of a 2.3-MVA Commercial Grid-Following Inverter via Frequency-Domain and Time-Domain Data," *IEEE Trans. Energy Convers.*, vol. 36, no. 3, pp. 2463-2472, Sept. 2021.

[3] U. Karaagac, J. Mahseredjian, S. Jensen, R. Gagnon, M. Fecteau, and I. Kocar, "Safe Operation of DFIG-Based Wind Parks in Series Compensated Systems," *IEEE Trans. Power Deliv.*, pp. 709-718, 2018.

[4] L. Meng, U. Karaagac, A. Pavani, J. Mahseredjian, and K. Jacobs, "Examination of EMT-Type Impedance Scanning Techniques for Small Signal Stability Assessment of Inverter Based Resources," *IEEE Trans. Power Delivery*, pp. 1-13, 2025.

[5] K. Jacobs, Y. Seyedi, L. Meng, U. Karaagac, and J. Mahseredjian, "A comparative study on frequency scanning techniques for stability assessment in power systems incorporating wind parks," *Electric Power Systems Research*, vol. 220, p. 109311, July 2023.

[6] M. Lwin, R. Kazemi, and D. Howard, "Frequency Scan Considerations for SSCI Analysis of Wind Power Plants," in *2019 IEEE Power & Energy Society General Meeting (PESGM)*, Aug. 2019, pp. 1–5.

[7] S. Shah, P. Koralewicz, R. Wallen, and V. Gevorgian, "Impedance Characterization of Utility-Scale Renewable Energy and Storage Systems," in *2019 IEEE Energy Conversion Congress and Exposition (ECCE)*, Baltimore, MD, USA: IEEE, Sept. 2019, pp. 2609-2616.

[8] Y. Zhu, Y. Zhang, and T. C. Green, "Injection Amplitude Guidance for Impedance Measurement in Power Systems," *IEEE Transactions on Power Electronics*, vol. 38, no. 6, pp. 6929-6933, June 2023.

[9] H. Alenius, R. Luhtala, and T. Roinila, "Amplitude Design of Perturbation Signal in Frequency-Domain Analysis of Grid-Connected Systems," *IFAC-PapersOnLine*, vol. 53, no. 2, pp. 13161-13166, 2020.

[10] Modern Control Engineering, 5th ed. Upper Saddle River, NJ, USA: Prentice Hall, 2010.